remote sensing

MDPI

Article

A Multi-Objective Modeling Method of Multi-Satellite Imaging Task Planning for Large Regional Mapping

Yaxin Chen, Miaozhong Xu, Xin Shen *, Guo Zhang, Zezhong Lu and Junfei Xu

State Key Laboratory of Information Engineering in Surveying, Mapping and Remote Sensing, Wuhan University, Wuhan 430079, China; chenyaxin@whu.edu.cn (Y.C.); Mzxu6319@whu.edu.cn (M.X.); guozhang@whu.edu.cn (G.Z.); luzezhong@whu.edu.cn (Z.L.); junfei_xu@whu.edu.cn (J.X.)

* Correspondence: xinshen@whu.edu.cn; Tel.: +86-186-2780-1540

Received: 18 December 2019; Accepted: 19 January 2020; Published: 21 January 2020

Abstract: Regional remote sensing image products are playing an important role in an increasing number of application fields. Aiming at multi-satellite imaging task planning for large-area image acquisition, this paper proposes a multi-objective modeling method. First, we analyzed the core requirements of regional mapping for multi-satellite imaging mission planning: Full coverage of the target area and low consumption of satellite resources. Second, an optimization model with two objective functions, namely the maximum target area coverage and minimum satellite resource utilization, was established. Using the selection of imaging strips and their swing angles as two types of decision variables, the regional decomposition and satellite resource allocation were integrated into the planning model. Third, two efficient algorithms, Vatti and non-dominated sorting genetic algorithm (NSGA-II), were used for objective function calculation and model solving, respectively. Finally, the experiments used Hubei, Finland, and Congo as the target areas and GF1, GF6, ZY1-02C, and ZY3 as imaging satellites to verify the modeling method proposed in this paper. The experiments showed that the proposed multi-objective modeling method could complete the coverage of regional targets with fewer satellite resources and improve the satellite application efficiency significantly.

Keywords: regional mapping; multi-satellite imaging mission planning; multi-objective optimization model; NSGA-II

1. Introduction

Regional mapping refers to the process of obtaining remote sensing images through planning satellites and generating complete regional images through geometric and radiation processing of remote sensing images [1]. Regional remote sensing image products are widely used in many fields, such as urban planning and construction [2], land census and national condition monitoring [3], agriculture and forestry change and monitoring [4], ecological environment assessment and monitoring, emergency response and rescue [5,6], and national defense security. With the development of imaging satellites, relevant organizations and departments in the world are committed to producing regional imaging products for a city, a country, or even the world.

Although considerable work has been done on the application and production of regional remote sensing images [7], there is less focus on using earth observation satellites to obtain regional images efficiently. The basic process of regional mapping should include the following steps: (1) Satellite imaging task planning to obtain a satellite imaging scheme; (2) obtaining remote sensing image data according to imaging scheme; and (3) generating regional digital orthophotos and other regional image products through image preprocessing, image matching, block adjustment, orthophoto correction,

fusion, uniform light and color, mosaic, and other processes. Among these steps, imaging task planning involves reasonably allocating satellite resources and imaging time to earth observation tasks on the precondition of satisfying complex constraints [8]. It is the basic step of regional mapping, which is an important guarantee for efficient and high-quality acquisition of regional image products [9].

Regional images have traditionally been obtained using a single satellite. However, with the rapid growth in the number of remote sensing satellites and the expanding application area of regional remote sensing image products, users are increasingly demanding timeliness in regional image acquisition [10], which may be annual, seasonal, or even monthly. In addition, because of the limited swath width of high-resolution imaging satellites and limited number of satellite crossings within a short period of time, it is almost impossible to meet the timeliness requirements of regional image acquisition using a single satellite to obtain regional images. Therefore, it is necessary to use multiple satellites with the same sensor type and similar spatial resolution for common imaging, for ensuring quicker access to space resources [11,12], as shown in Figure 1a. The practical problem of scheduling multiple satellites for regional mapping is more complicated than when using a single one. Although satellites are tied to predefined orbital paths, the maneuverability of satellites can provide more frequent opportunities for observing the target area, resulting in a larger number of combination schemes between satellite resources to cover regional targets. Therefore, for regional mapping, choosing the "best" combination scheme to reasonably allocate satellite resources can ensure that satellites can cooperate with each other to efficiently complete regional image acquisition, which is a complicated process. In addition, if satellites are not properly planned, some parts of the target area will be repeatedly observed, and other parts will not be covered by any image [13], as shown in Figure 1b.

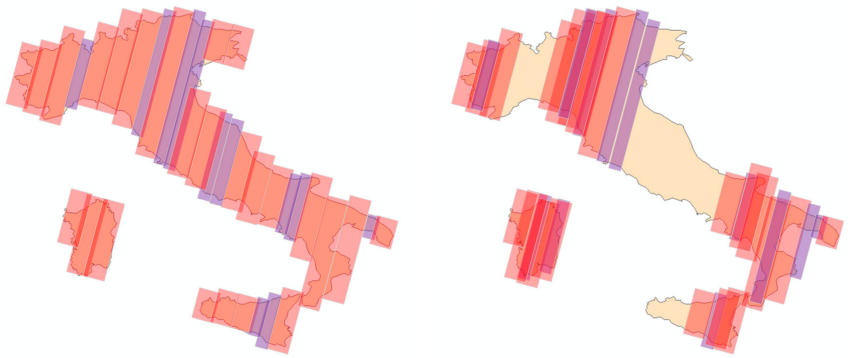

(**a**) (**b**)

Figure 1. Italy covered by swaths from different satellites. (**a**) Swaths planned by using "maximal-coverage" criteria; (**b**) No planned swaths.

The basic process of satellite task planning for regional mapping involving multiple imaging satellites includes the following steps: First, accepting the user's needs and selecting feasible satellite resources according to the requirements of the sensor type and spatial resolution; then, building the mathematical model for imaging task planning and solving the model to obtain the satellite task planning scheme; and finally, evaluating the scheme and formulating the multi-satellite imaging task planning scheme. Model building is the basis of solving the problem of imaging satellite mission planning [14] and provides the mathematical expression of user and planning requirements. The correctness and accuracy of the model determine the reliability and effectiveness of the optimization results [15]. According to the requirements of regional mapping, the core requirement of imaging satellite mission planning is to use as few satellite resources as possible to ensure full coverage of the target area. Therefore, in planning and modeling of regional mapping tasks, the core requirement must be considered.

At present, there are few studies on multi-satellite task planning for regional mapping, we can learn from the task planning for regional target. Research on models for multi-satellite imaging mission

planning involving a regional target is less than that regarding spot targets, which can be covered by a single strip of satellites. A general approach to the problem consists of two steps. The first step is to decompose the target region according to certain rules into a series of subtasks, which are called spot targets. The second step is to select a subset of these spot targets and allocate them to specific satellites using various models and algorithms. In other words, this approach divides the problem of satellite scheduling for regional target into two sub-problems, i.e., the decomposition of the target area and optimization of scheduling models. Typical target decomposition methods include the grid method and the strip method. The grid method divides the target region into a collection of point targets. Rivett [16] studied multiple satellites with same-performance radar sensors to complete regional target mission planning within a user-defined time. By gridding regional targets, an integer planning model with maximum coverage as the objective function was established, and eight satellites were sufficient to complete the observation tasks that previously required 16 satellites. Ruan [17] proposed a method for creating a grid space based on the Gaussian projection of the regional target and updated rules of the grid space state, and provided a coverage calculation method based on grid space state statistics. On this basis, a mathematical model for the reconnaissance satellite scheduling problem was established, which optimizes the two objective functions of the maximum observation benefit and minimum observation cost in a hierarchical priority manner. Shao [18] decomposed regional targets into multiple point targets using a grid of equal latitude and longitude and established a planning model with the maximum total revenue and maximum number of completed tasks as objective functions. The digital elevation model and moving target on the ground are obtained simultaneously using the satellite formation flight system.

The strip method decomposes the target area into a rectangular strip that can be completely covered by a single transit of the satellite. Li [19] aimed to solve the large-area target multi-satellite collaborative earth observation mission planning problem by discretizing the imaging swing angles of each satellite to generate candidate imaging strips for regional pre-decomposition; then, considering the maximum coverage of the target area as the objective function, he proposed a dynamic segmentation method for the target area. Liu [20] considered the orbit characteristics of satellites and observation capabilities of remote sensors and carried out strip drawing at a certain granularity angle according to the satellite trajectory and established a dynamic decomposition method for regional targets. A multi-satellite collaborative observation scheme for regional targets based on MapX was proposed. He [21] established a five-tuple subtask set mainly based on the time window and swing angle. Through dynamic decomposition, the regional target was decomposed into a series of candidate subtasks with different satellites and swing angles. By establishing a planning model with a coverage function as the objective function, the planning problem of regional targets in the two-satellite mode was solved.

Scheduling models can be divided into single-objective and multi-objective models according to the number of objective functions in the models. For the single-objective model, He [22] designed a multi-satellite collaborative scheduling framework for imaging tasks under emergency conditions. The multi-satellite collaborative scheduling problem was decomposed into two tasks: Task sequencing and resource matching. The constraint satisfaction model of the problem was constructed with maximization of task revenue as the optimization objective. Shi [23] established an imaging satellite mission planning model with minimum satellite resource consumption as the objective function; the model satisfies the imaging time window constraint, imaging strip overlap ratio constraint, and coverage constraint. By solving the model with an approximate algorithm, the long-term optical remote sensing imaging task planning problem for large-area targets at low and middle latitudes is solved. Considering mission planning for satellite image acquisition in disaster-stricken areas of large regions, Liu [24] considered the possible discontinuities in the disaster-stricken areas, assigned different weights to different regions, and established a satellite mission planning model with optimal spatial resolution as the objective function. Given a set of satellites and a mission time frame, Perea [25] decomposed regional targets using a set of possible sensor angle positions for satellites and established a linear programming model; the minimum image acquisition cost was set as the objective function

and the coverage of all sub-regions in at least one acquisition was the constraint. Further, in applying satellite imaging to early warning hydrological models, Estefanía [26] assigned different weights to area coverage, request priority, request mode, and swath usage and established a single-objective optimization model.

As for multi-objective models, to solve the problem of large-area multi-satellite imaging scheduling, Li [27] divided the target area using the equal distance grid method; then, he established the constraint satisfaction model with the maximum coverage of the target area, minimum overlap of the imaging strip, and shortest imaging time as the objective functions. Niu [28] used the multi-satellite large-area mission planning to solve the emergency response problem during natural disasters. First, the imaging strip sequence was obtained by discretizing the satellite swing angle to decompose the regional targets. Then, according to different application scenarios, through different combinations of four objective functions, namely the maximum coverage, shortest completion time, highest spatial resolution, and minimum average swing angle, an integer programming model was established to find the optimal combination of strips. For the high dynamics and high time sensitivity of emergency observation missions, Cui [29] established a multi-objective dynamic programming model with three objective functions for maximizing the observation mission priority and mission revenues and minimizing the waiting time.

However, there are some shortcomings in the task planning model based on the above methods. First, multi-satellite mission planning for regional areas involves decomposition of the target area and optimization of scheduling models. These two steps should be interconnected. Although scheduling models find the "best" subset from the set obtained through decomposition of the target area, optimization of the scheduling model has no effect on the decomposition of target areas. In addition, the planning results are highly dependent on the accuracy of region decomposition, but the accuracy of region decomposition is inconsistent with the efficiency of the model solution. Second, in terms of the scheduling models, the single-objective model with only the coverage rate as the objective function ignores the problem of overlapped observation caused by multiple satellites; in such cases, it is easy to waste satellite resources and difficult to meet the multi-satellite regional target mission planning requirements. Multi-objective modeling can consider more than one objective function and obtain a more reasonable planning solution. However, if the model has too many objective functions, it would be difficult to obtain the optimal solution, and correlations between objective functions must be avoided. To develop the model for multi-satellite regional mapping planning, we must construct the objective function according to the core requirement of the mission, which is to use minimum satellite resources and ensure full coverage of regional targets efficiently and quickly.

In this study, we developed a multi-objective optimization model to solve the multi-satellite task planning problem for large-area mapping. Starting from the two core requirements of multi-satellite regional mapping, namely full coverage of target areas and low consumption of satellite resources, we established a multi-objective optimization model with maximum area coverage and minimum satellite resource consumption as the objective functions. By choosing whether to select the imaging strip and swing angle of the imaging strip as decision variables, decomposition of the target areas and optimization of scheduling models are performed simultaneously. The model is solved using the non-dominated sorting genetic algorithm(NSGA-II) and the effective coverage area in the objective function is calculated using the polygon Boolean operation Vatti algorithm, which effectively improves the speed of obtaining the optimal solution of the model. Finally, taking three regions, Hubei, Finland, and The Democratic Republic of the Congo (Congo for short in this paper) with different latitudes, sizes, and shapes as examples, the experiments verified that the proposed multi-objective optimization model used less satellite resources for complete coverage of the regional targets within the user-defined time. The proposed task planning model for large-area multi-satellite imaging meets the needs of regional mapping.

The remainder of the paper is organized as follows. In Section 2, the modeling process of the multi-satellite mission planning for large-area mapping is introduced considering three aspects:

Simplifying the planning process, model preparation, and model construction, and the method of model solving and the method of calculating the objective function are given. In Section 3, we describe the experiments performed using three different target areas as examples, compare two commonly used task schemes, and present the experimental results and analyses. The proposed method is discussed in Section 4. Finally, the conclusions of the study are given in Section 5.

2. Proposed Methods

To realize the rapid mapping of a large regional objective and meet the needs of different departments in terms of regional products and their updates, we developed a multi-satellite task planning multi-objective model for regional mapping. First, a multi-objective task planning model with two types of decision variables, two objective functions, and two constraints was established by simplifying the planning process and analyzing the main user needs and task planning needs of regional mapping. Then, the model was solved using the multi-objective genetic algorithm NSGA-II to obtain a multi-satellite mission planning plan for regional targets. The flowchart of the multi-satellite mission planning scheme proposed in this paper is illustrated in Figure 2.

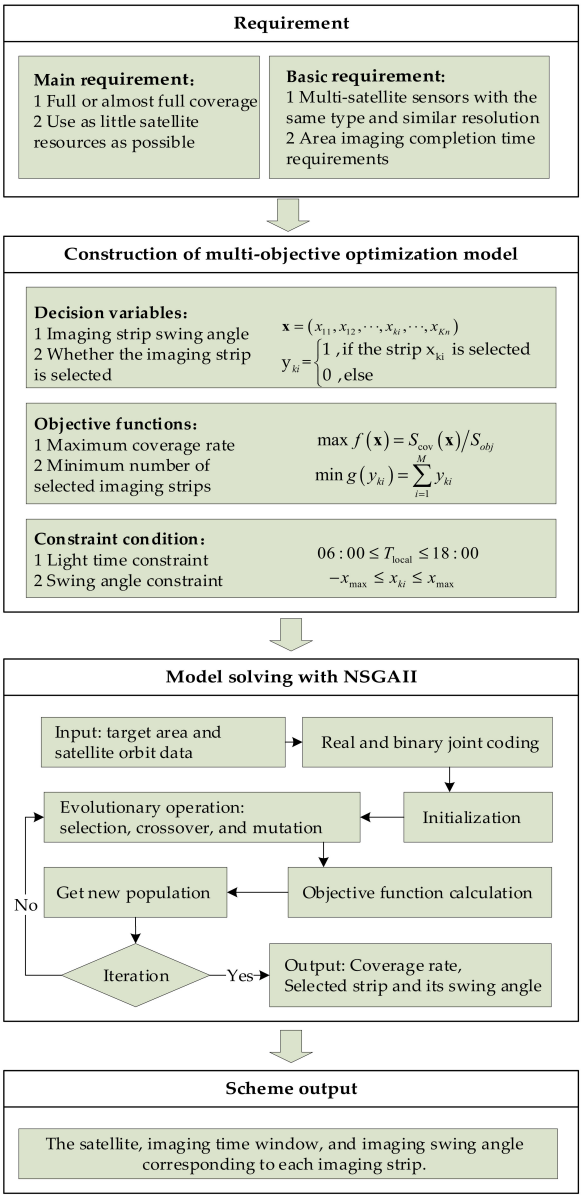

Figure 2. Flowchart of the multi-satellite mission planning scheme for large-area mapping.

2.1. Multi-Objective Optimization Model Construction

2.1.1. Planning Process Assumptions and Simplifications

As multi-satellite mission planning has proven to be a non-deterministic polynomial(NP-hard) problem. To facilitate modeling, this study makes appropriate assumptions and simplifies the multi-satellite area mapping planning process before modeling, as is the case in other existing studies. The simplification of the planning process considers major factors in planning issues and ignores minor factors. For different planning problems, the focus of the assumptions on the constraints is also different [30]. For multi-satellite large-area mapping, we used the following assumptions and simplifications:

1. Regional mapping can be regarded as a single task, and each satellite only performs this task when executing the shooting scheme, without considering other tasks;
2. For regional targets, imaging can be performed during satellite transit under the constraints of lighting;
3. As the swing angle of a satellite is a fixed value each time it passes through, and it only crosses once in a circle, the satellite maneuver adjustment time is assumed to meet the imaging conditions.
4. Changes in image spatial resolution caused by different swing angles are considered acceptable within a certain range;
5. The satellite is assumed to meet storage and energy constraints;
6. Each satellite is assumed to have only one payload; and
7. It is assumed that weather factors satisfy imaging conditions.

2.1.2. Preparation for Model Construction

The planning model is a mathematical expression of user requirements and task planning. To establish a simple, accurate, and effective multi-satellite task planning model for large-area targets, detailed analyses and decomposition of user requirements and task planning requirements are performed before modeling.

For large-area mapping, user needs mainly include the target imaging area, completion time, acquisition image type (such as optical, SAR, or hyperspectral), and spatial resolution of the regional product. Correspondingly, the task planning requirements include the sensor requirements of multiple satellites with the same sensor type and similar spatial resolution, coverage requirements for ensuring full coverage or almost full coverage of the regional target within the specified time, and satellite resource requirements for completing the regional imaging task with as few satellite imaging strips as possible within the specified time.

These requirements can be translated into different components of a multi-objective model for large-area target multi-satellite mission planning. Model constraints can be determined based on satellite sensor types, including swing angle maneuver constraints and light time constraints. Model inputs can be determined based on the imaging area, imaging completion time, and satellite sensors, including the imaging area boundary coordinates, and satellite orbits within a specified time. Model decision variables can be determined based on satellite resource requirements and model inputs, including the selection of imaging strips and the swing angle of each imaging strip. Model objective functions can be determined based on satellite resource requirements and coverage requirements, including the maximum coverage rate and minimum number of imaging strips. The transformation of the user requirements and mission planning requirements to a multi-objective model for multi-satellite mission planning in imaging large-area targets is shown in Figure 3.

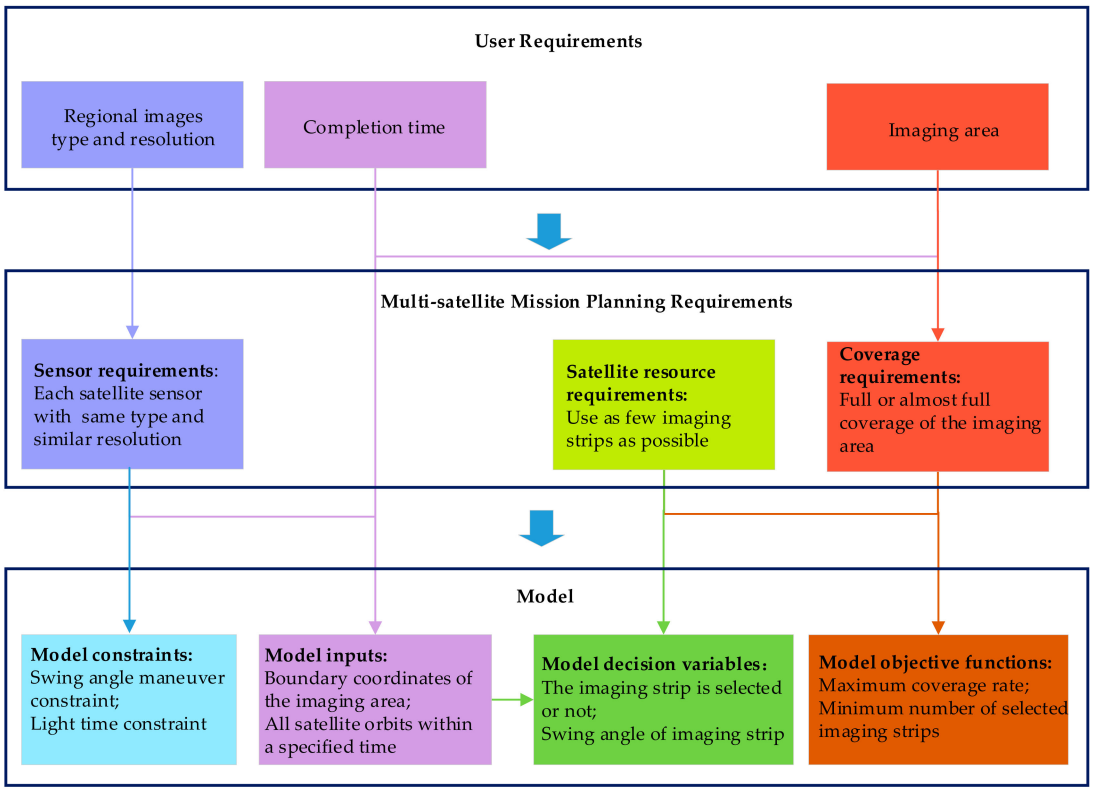

Figure 3. Transformation from requirements to planning model.

2.1.3. Model Construction

Based on the above assumptions and simplification of the planning process for multi-satellite large-area mapping and modeling preparation, the specific mathematical expression of the regional target multi-satellite task planning model established in this study is as follows:

● Decision variables

Expression of decision variable 1:

$$\mathbf{x} = (x_{11}, x_{12}, \cdots, x_{ki}, \cdots, x_{Kn}). \tag{1}$$

Decision variable **x** is the set of swing angles of all satellite imaging strips, with a length of M. x_{ki} is the swing angle of the imaging strip when satellite k passes through the target area for the ith time. x_{ki} is a continuous double variable. Through optimizing x_{ki}, the ith imaging strip of satellite k can be obtained to complete the regional target decomposition.

Expression of decision variable 2:

$$y_{ki} = \begin{cases} 1\text{, if the strip } x_{ki} \text{ is selected} \\ 0\text{, else} \end{cases}. \tag{2}$$

Decision variable y_{ki} represents whether the strip with swing angle x_{ki} is selected. If it is selected, $y_{ki} = 1$; otherwise, $y_{ki} = 0$. y_{ki} is a binary variable. Using y_{ki}, it can be determined whether the ith strip of satellite k participates in imaging, and then the satellite resource allocation is completed.

● Objective functions

Expression of objective function (1):

$$\max f(\mathbf{x}) = \frac{S_{\text{cov}}(\mathbf{x})}{S_{obj}}. \tag{3}$$

Objective function (1) ensures the maximum coverage rate of the imaging area. $S_{\mathrm{cov}}(\mathbf{x})$ represents the effective coverage area of the imaging strip and S_{obj} represents the target area.

Expression of objective function (2):

$$\min g(y_{ki}) = \sum_{i=1}^{M} y_{ki}. \tag{4}$$

Objective function (2) ensures the minimum number of imaging strips, that is, the minimum consumption of satellite resources.

● Constraints

Expression of constraint 1:

$$06:00 \le T_{\mathrm{local}} \le 18:00, \tag{5}$$

where T_{local} is the local time of the target. Constraint 1 represents the imaging strip meeting the illumination time constraint, which is from 06:00 to 18:00 local time in the target imaging area.

Expression of constraint 2:

$$-x_{\max} \le x_{ki} \le x_{\max}, \tag{6}$$

where $x_{\max}$ is the maximum swing range of the satellite sensor, taking the positive value as the left- side sway in the flight direction and the negative value as the right-side sway. Constraint 2 represents different satellites meeting the maximum swing angle constraint.

The multi-objective optimization model proposed in this paper has the following characteristics:

1. Taking the swing angle of the strip and selection of the strip as the decision variables, regional decomposition and resource allocation are integrated into the planning model. A multi-satellite planning scheme that takes into account both the coverage rate and satellite resource utilization can be directly obtained by solving the model, which simplifies the planning process.
2. It reduces the consumption of satellite resources while meeting the coverage of user needs.
3. The two objective functions are mutually constrained, and a set of non-dominated solutions can be obtained to meet the decision needs of different preferences.

2.2. Model Solving

2.2.1. Model Solving Based on the NSGA-II Algorithm

At present, there are three representative methods to solve the multi-objective model: strength pareto evolutionary algorithm (SPEA2) [31], NSGA-II [32], and pareto envelope-based selection algorithm II (PESA-II) [33]. Other algorithms are mostly improvements based on these. Zheng [34] analyzed the above three model solving methods using five benchmark problems: DTLZ1, DTLZ2, DTLZ3, DTLZ4, and DTLZ5. Among them, NSGA-II shows the best performance in terms of the distribution of solution sets and solution efficiency. In terms of convergence, when there are many objective functions, NSGA-II has a relatively poor convergence; however, when there are only two objective functions, NSGA-II has a similar performance to SPEA2 and PESA-II. Therefore, this study used NSGA-II to solve the proposed multi-objective model.

The steps for solving the multi-objective model of multi-satellite task planning for large-area targets are as follows:

1. Coding. Real variable encoding: The chromosome length, M, is the sum of the imaging strips of all imaging satellites. Gene is the swing angle of each imaging strip. Binary variable code: The length is the same as the real variable code. If the strip is selected, the corresponding gene is 1; otherwise, it is 0. The encoding is shown in Figure 4.
2. Initialization. Initialize the parent population and number of generations of evolution. In this study, the population size was set to 160, and the number of generations of evolution were set to 200, 300, and 2000, respectively, according to the three target areas.

3. Perform selection, crossover, and mutation operations on the parent population to produce the offspring population. In this study, the crossover rate of real variables was set to 0.7; the mutation rate of real variables was 0.01; the crossover distribution index was 10; the mutation distribution index was 12; the crossover rate of binary variables was 0.7; and the mutation rate of binary variables was 0.01.
4. Calculation of the objective functions.
5. The parent and offspring populations were merged, and new populations were generated by non-dominated sorting and the individual crowding calculation of the merged population.
6. Determine whether the iteration termination conditions were met; if the conditions were met, the planning scheme was output; if not, we repeated step 3.

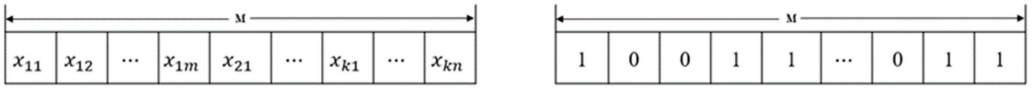

(**a**) (**b**)

Figure 4. Gene coding of decision variables. (**a**) Real swing angle coding; (**b**) Binary-selected stripe coding.

2.2.2. Calculation of Objective Function 1

1. Acquisition of imaging strips

Obtaining imaging strips mainly uses the position (P_X, P_Y, P_Z) and velocity (V_X, V_Y, V_Z) of satellites at the beginning and end of the imaging time, which can be extrapolated from satellite orbit data. Then, according to the field of view angle of the satellite and swing angle of the sensor during imaging, the intersection point between the line of sight and the ground surface can be calculated. The polygon formed by these intersections (A,B,C,D) is the imaging strip. Because the calculation formula is complex and is not main research focus of this study, the calculation formula is not presented in detail; only the imaging schematic diagram is given, as shown in Figure 5.

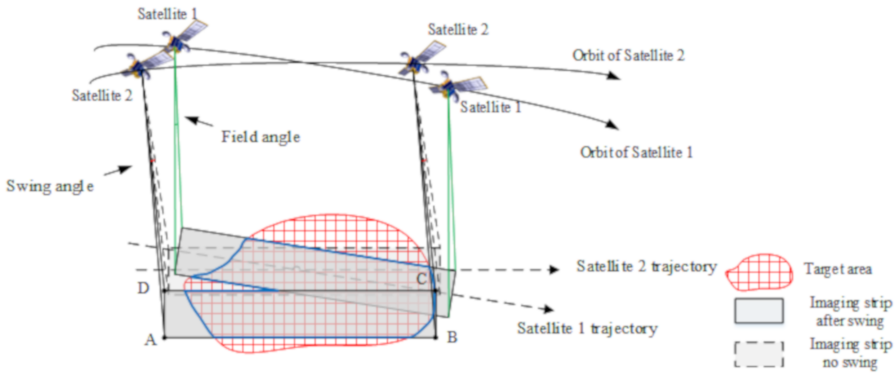

Figure 5. Imaging strips from different satellites and their coverage.

2. Calculation of the coverage area

When using the NSGA-II algorithm to solve the model, the objective function must be calculated in each individual generation. The number of calculations is very large, which is equal to the product of the number of generations of evolution and the population size. For the coverage rate calculation, i.e., the first objective function, the common method is the grid statistical method based on grid decomposition. However, the calculation accuracy of the grid method depends on the size of the grid. The smaller the grid, the higher the calculation accuracy, but the larger the calculation cost; hence, it cannot meet the calculations requirements. It is difficult for the grid method to achieve a good balance between the calculation accuracy and calculation cost. Therefore, in this study, we used the Vatti

algorithm [35,36] to solve the problem. According to certain rules, the Vatti algorithm determines that either the left or the right side should be selected as the edge of the area covered by strips at any intersection, which may be formed by an imaging strip and other imaging strips or an imaging strip and the target area. As shown in Figure 5, the area marked has a a blue boundary. The Vatti algorithm uses the coordinates of the boundary points on the covering polygon to calculate the area rather than the grid statistics, so the results are more accurate and efficient. More information about the Vatti algorithm is provided elsewhere [35].

3. Experiments and Analyses

3.1. Experimental Data

3.1.1. Imaging Satellite

To ensure that the images acquired by different satellites can be stitched into complete regional images, four optical satellites with 2-m resolution sensors were selected for regional imaging in the experiment. They were GF1, GF6, ZY1-02C, and ZY3. Some parameters of the satellites and sensors are listed in Table 1.

Table 1. Satellite and sensor parameters.

Satellite	GF1	GF6	ZY1-02C	ZY3
Agency	China Aerospace Science and Technology Corporation			
Launch time	20 April 2013	2 June 2018	22 December 2011	9 January 2012
Orbit Type	Repeat sun-synchronous orbit			
Orbital Altitude (km)	645	645	780	506
Return Period(days)	41	41	55	59
Swing Ability	±35°	±35°	±25°	±32°
Payload Imaging Width (km)	60	45	54	51
Half Field Angle	2.67°	3.99°	1.98°	2.88°

3.1.2. Imaging Areas

To verify the effectiveness of the planning model proposed in this paper, the following three regions with different latitudes, shapes, and sizes were selected as the target regions: Hubei, China; Finland; and Congo. The distribution of the three regions is shown in Figure 6, and the basic parameters of the target regions are given in Table 2.

Figure 6. Distribution of target regions.

Table 2. Parameters of target regions.

Region	Latitude	Shape	Area (km^2)
Hubei	middle	approximately flat rectangle	about 185,900
Finland	high	approximate high rectangle	about 338,000
Congo(K)	low	approximately square	about 2.345 million

3.1.3. Imaging Time

In this experiment, the time of regional imaging ranged from 8 September 2019 to 20 September 2019, a total of 13 days. As the four imaging satellites selected were optical satellites, the imaging time constraint was set from 06:00 to 18:00 local time in the selected area.

According to the imaging satellite, target area, mission completion time, and orbit parameters of the satellites, the visible time window of the satellites and target regions can be calculated. The orbit parameters of each satellite can be obtained from https://celestrak.com/. To facilitate optimization of the swing angle of the imaging strip in this study, the visible time window was appropriately extended. Table 3 mentions the number of visible time windows of each satellite to each target region, that is, the number of satellite transit orbits. The expanded visible time windows of each satellite to the regional targets are listed in Appendix A.

Table 3. Number of satellite transit orbits.

Satellite	Hubei	Finland	Congo
GF1	3	9	10
GF6	4	9	10
ZY1-02C	4	10	10
ZY3	3	9	10
total	14	37	40

3.2. Experimental Results and Analyses

3.2.1. Experimental Results

Figures 7–9 show the imaging results obtained using different modeling methods for Hubei, Finland, and Congo, respectively. In each figure, the green strip represents the imaging strip of GF1, the blue strip represents that of GF6, the pink strip represents that of ZY1-02C, and the yellow strip represents that of ZY3. Among them, Figures 7a, 8a and 9a show the satellite trajectories corresponding to the visible time window. The red oblique solid line indicates the trajectories of the four satellites for each target area, and the green solid line (GF1), blue solid line (GF6), pink solid line (ZY1-02C), and yellow solid line (ZY3) indicate the trajectory of each satellite after the visible time window is extended. Figures 7b, 8b and 9b present the imaging results of three target areas covered by the satellites during vertical imaging, that is, the imaging results when the swing angles are zero. Figures 7c, 8c and 9c present the optimized imaging results of the three regions obtained using the model proposed in [37], which uses only the coverage as the objective function. Figures 7d, 8d and 9d present the optimized imaging results of the three regions when the model was constructed using the method proposed in this paper.

Table 4 presents a comparison of the number of strips and coverage rate required by different modeling methods to complete regional imaging. Table 5 provides the optimization results of the swing angles of the effective imaging strips when the model only used the coverage as the objective function. Table 6 gives the optimization results of the swing angles of the selected imaging strips when the multi-objective model proposed in this paper was used. The gray background in Tables 5 and 6 is the swing angle of the effective imaging strip or the selected imaging strip. Table 7 presents all

the non-dominant imaging planning schemes obtained using the multi-objective optimization model proposed in this paper.

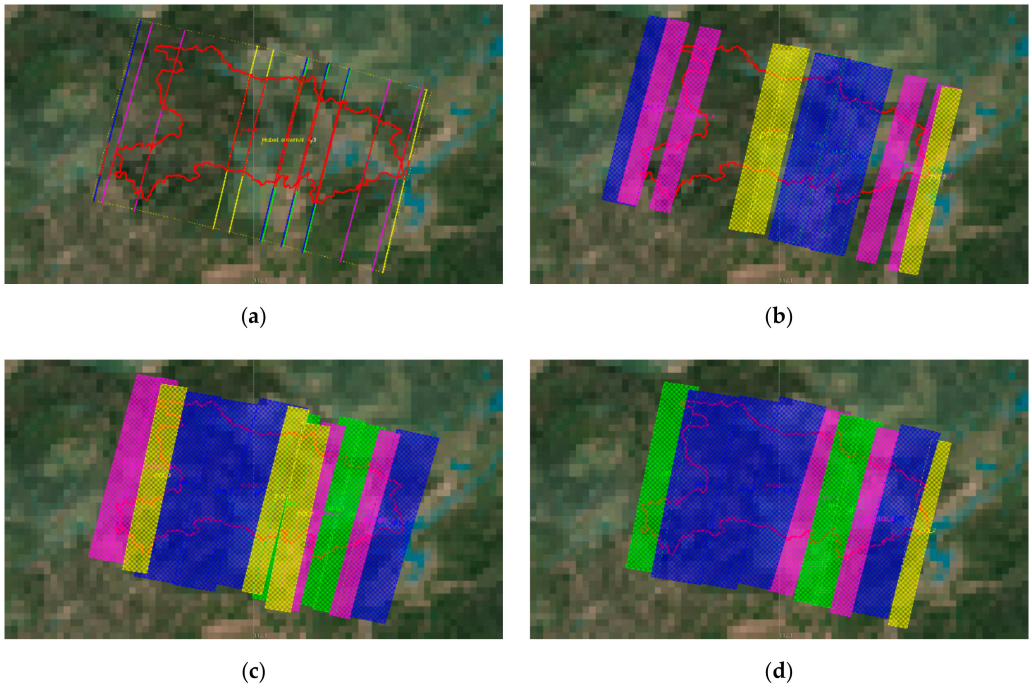

(**a**) (**b**)

(**c**) (**d**)

Figure 7. Mission planning results obtained using different modeling methods in Hubei. (**a**) Satellite trajectories; (**b**) satellite vertical imaging results without optimization; (**c**) satellite optimized imaging results when the model has only one objective function; and (**d**) satellite optimized imaging results when the multi-objective modeling method proposed in this paper was used.

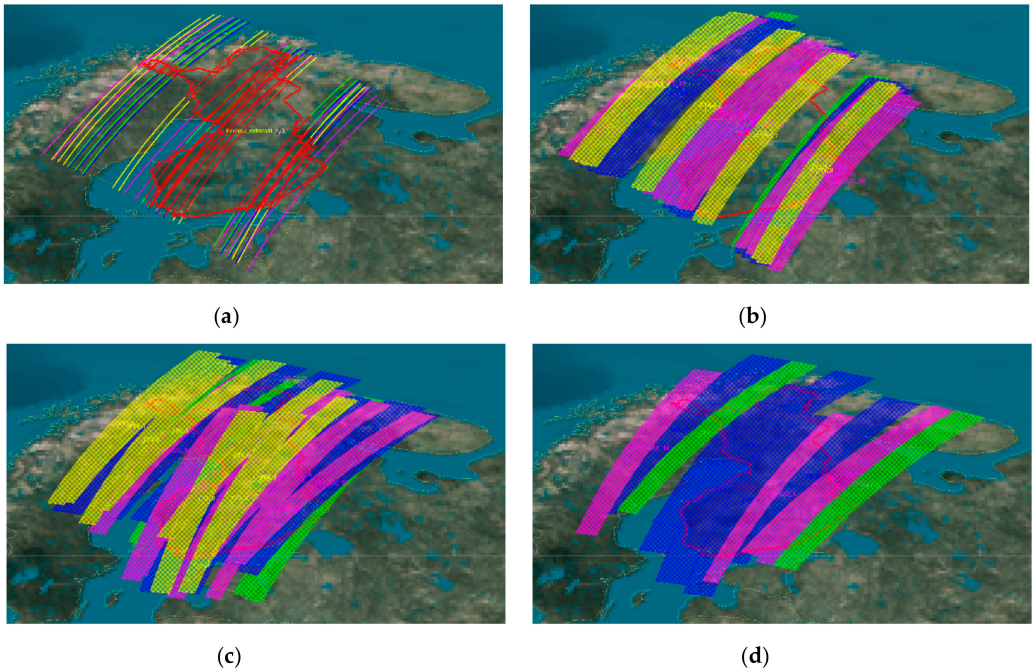

(**a**) (**b**)

(**c**) (**d**)

Figure 8. Mission planning results obtained using different modeling methods in Finland. (**a**–**d**) Same as Figure 7.

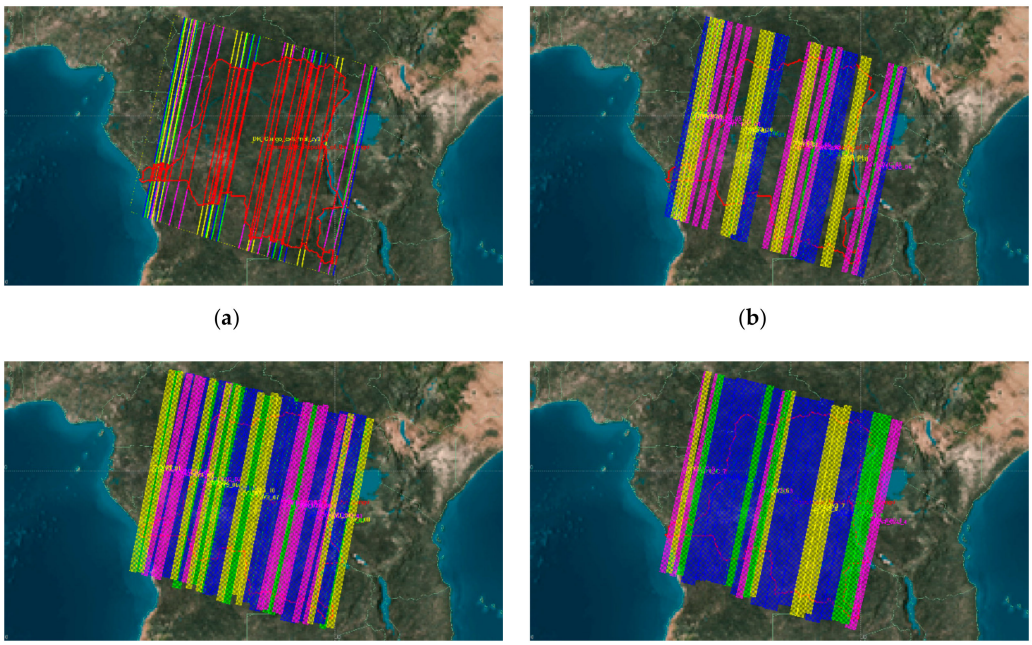

Figure 9. Mission planning results of different modeling methods in Congo: (**a**–**d**) Same as Figure 7.

Table 4. Number of imaging strips and coverage rate obtained with different modeling methods.

Target Region	No Optimization		Optimization Model with Only One Objective Function		Optimization Model Proposed in this Paper	
	Effective Strips	Coverage Rate	Effective Strips	Coverage Rate	Effective Strips	Coverage Rate
Hubei	14	61%	14	100%	10	100%
Finland	37	79.64%	31	100%	12	100%
Congo	40	66.2%	39	99.95%	25	99.97%

Table 5. Swing angle of each satellite imaging strip in model with only one objective function.

Target Region	Swing Angle							
	GF1		GF6		ZY1-02C		ZY3	
Hubei	−9.52	9.45	−23.66	24.08	0.15	−2.80	−11.71	26.30
	−9.73		27.09	−29.12	16.25	6.85	28.86	
Finland	−24.50	−4.76	−20.58	−9.38	20.25	2.60	−4.16	−16.26
	1.82	−7.35	−28.00	5.32	−9.40	−21.55	10.24	−7.49
	16.45	5.18	−21.70	24.78	24.25	19.60	−9.02	29.70
	−5.95	31.50	−8.33	−22.68	9.80	23.40	19.07	3.46
	−16.38		14.14		7.35	−11.30	−14.40	
Congo	5.25	28.42	−10.15	−28.56	9.65	−19.05	7.23	3.90
	32.13	20.79	−21.00	20.02	−24.15	17.60	9.86	14.66
	3.57	6.65	34.51	8.33	−18.15	−1.20	27.97	−28.61
	6.44	−27.72	−34.72	6.58	22.65	15.15	−14.46	25.60
	6.30	−30.59	−28.91	−15.33	4.40	−8.60	−23.04	−29.12

Table 6. Swing angle of each satellite imaging strip in the proposed multi-objective optimization model.

Region	Swing Angle							
	GF1		GF6		ZY1-02C		ZY3	
Hubei	30.22	1.24	−19.20	31.86	−22.30	−1.56	−14.90	−19.93
	0.71		20.38	−28.06	11.22	−22.47	3.19	
Finland	−1.53	19.61	−20.97	−14.41	8.98	7.13	27.52	11.78
	−22.63	−3.58	23.27	−15.65	−23.58	−21.95	7.49	11.18
	−8.53	19.69	6.20	20.42	12.41	7.64	−31.07	2.76
	−7.69	24.88	0.52	11.65	−21.83	−19.18	20.24	−29.55
	−29.50		−1.84		−3.38	23.13	28.70	11.78
Congo	26.67	−7.77	32.82	−33.83	−2.64	−24.69	4.70	−25.99
	−33.14	−13.20	−32.41	35.00	−4.51	16.00	12.55	−30.45
	6.43	−31.04	35.00	−33.12	18.24	−5.91	6.71	28.40
	−8.67	0.02	−23.91	−16.50	0.93	−5.15	29.78	−11.79
	11.49	−34.98	0.65	31.12	16.72	0.42	5.31	17.53

Table 7. Different satellite imaging planning schemes determined using the multi-objective optimization model proposed in this paper.

Target Region	Number of Imaging Strips	Coverage Rate	No. of Imaging Strips	Coverage Rate	No. of Imaging Strips	Coverage Rate	No. of Imaging Strips	Coverage Rate
Hubei	1	24.13%	4	75.83%	7	95.62%	10	100.00%
	2	46.49%	5	83.69%	8	97.66%		
	3	62.14%	6	90.60%	9	98.94%		
Finland	1	30.33%	4	80.13%	7	95.16%	10	98.91%
	2	55.62%	5	87.54%	8	97.24%	11	99.80%
	3	72.55%	6	92.45%	9	98.53%	12	100.00%
Congo	1	11.59%	8	69.91%	15	94.79%	22	99.40%
	2	22.99%	9	75.53%	16	95.49%	23	99.74%
	3	32.96%	10	80.95%	17	96.07%	24	99.84%
	4	41.91%	11	86.00%	18	97.16%	25	99.97%
	5	50.77%	12	89.38%	19	98.20%		
	6	57.94%	13	91.88%	20	98.62%		
	7	64.29%	14	93.76%	21	99.05%		

3.2.2. Experimental Analyses

For Hubei, Figure 7a shows that the trajectory distribution of satellites is relatively uniform and almost "parallel," except for the three trajectories of GF1 and three trajectories of GF6 in the middle of Hubei. However, for Finland (Figure 8a) and Congo (Figure 9a), most trajectories are very concentrated, and some trajectories located in Finland also have "trajectory crossing". In addition, there are no satellite trajectories in some of the three regions. Figures 7b, 8b and 9b present the imaging results when the satellites do not perform swing imaging, which means only vertical imaging is performed. Furthermore, for the regional target, except for a part of the area that is only observed once, other areas were repeatedly observed, and some were not observed. It can be inferred from Table 4 that without model optimization, the coverage rate of the 14 imaging strips in Hubei is only 61%, that of the 37 imaging strips in Finland is only 79.64%, and that of the 40 imaging strips in Congo is only 66.2%. This is caused by the uneven distribution of satellite trajectories. The distribution of satellite trajectories determines the satellite resource consumption and completion of regional imaging. An overly concentrated distribution will waste satellite resources, and too sparse a distribution will not complete regional imaging. For mapping one area, it can be considered that repeated observations are not necessary. Therefore, if we do not effectively plan for each satellite, we will waste satellite resources and not be able to complete regional mapping within the specified imaging time.

Figure 7c, Figure 8c, and Figure 9c present the mission planning results for Hubei, Finland, and Congo, respectively, when the optimization model only uses the coverage as the objective function. Compared to the planning results without optimization, full coverage or almost full coverage of the three regions is achieved, and the image acquisition for regional mapping is completed within the specified time. In terms of satellite resource utilization, Hubei (Figure 7c) has fewer repeated observations and higher resource utilization. This is because of the moderate number and distribution of satellite trajectories in Hubei, located at middle latitudes. For Finland, it can be clearly seen that there is a large overlap of imaging strips, and wastage of satellite resources is serious. This is because of its high-latitude geographic location, and there are more observation opportunities in the same imaging time; that is, there are more imaging strips, and all imaging strips participate in optimizing imaging, which will inevitably cause significant resource redundancy. For the Congo, satellite resource utilization is better than that of Finland, as observed in Figures 8c and 9c; however, its area is approximately 12 times that of Hubei and 7 times that of Finland. Because of its huge base, there will be significant wastage of satellite resources.

Figures 7d, 8d and 9d present the results of multi-satellite mission planning in Hubei, Finland, and Congo when the multi-objective optimization model proposed in this paper is used. It can be seen that for the three regions, repeated observations are rare, and each imaging strip is indispensable. Compared to the optimization results of the single-objective model (Table 4), the multi-objective model proposed in this paper provides the same coverage, with a considerable reduction in the number of strips. For complete coverage of Hubei, the single-objective model needs 14 imaging strips while the multi-objective model only needs 10 imaging strips. For complete coverage of Finland, the single-objective model needs 31 imaging strips while the multi-objective model only needs 12 imaging strips. For Congo, the single-objective model can cover 99.95% with 39 imaging strips while the multi-objective model can cover 99.97% with only 25 imaging strips. In addition, from the results in Tables 6 and 7, it is evident that the multi-objective modeling method proposed in this paper can achieve full coverage of the three regional targets with less satellite resources.

For any multi-objective optimization model, its solution is a set of non-dominated solutions, not a single one. The above optimization result obtained using the multi-objective model is the one with the highest coverage rate. The different optimization schemes for the three target regions are listed in Table 7, and decision makers can choose different schemes according to their preferences.

4. Discussion

Effective scheduling of multiple satellites is one of the critical steps for regional mapping. Although the satellites are fixed in their own orbits, if satellite utilization is not properly planned, multiple overlapping images may be obtained for certain parts of the target area and some parts may not be covered. In terms of urban planning, if we do not develop an efficient satellite imaging scheme through satellite planning, to ensure complete imaging of an urban area, we have to extend the imaging time. However, for providing rapid response to natural disasters, it is necessary to obtain images of the affected area in a short time. The proposed method uses less resources to achieve coverage within a specified time, and the saved resources can be effectively utilized for satisfying other observation demands instead of being redundant. A general approach to multi-satellite mission planning for large regions consists of two steps: Decomposition of target areas and optimization of scheduling models. This approach is limited by the size of the grid or the stripe angle particle size, and the optimal solution search is limited to selecting solutions from the subset of the existing decomposition scheme, which is not conducive for finding optimal solutions. Our method can obtain the optimal imaging scheme and region decomposition scheme at the same time. Region decomposition and imaging scheme optimization are performed as synchronous processes rather than two independent steps. An effective target area is obtained by calculating the coordinates of the boundary points using the Vatti algorithm, which is more accurate than the grid statistical method. In addition, the proposed method can provide

a set of imaging schemes for decision makers to select from, as the multi-objective model can provide multiple non-dominated solutions.

In studies on multi-satellite regional observations, coverage is the most frequently considered requirement by researchers. In addition, imaging completion time, satellite resource optimization, and spatial resolution are also considered. The planning method basically selects one or more of these requirements to establish a constraint satisfaction model or a multi-objective model. There are many methods that convert multiple objectives into a single objective by using predefined weights. Nevertheless, in most cases, multiple requirements are independent and may even be contradictory; therefore, the solution is sensitive to the weight, and different weight allocation strategies may lead to different solutions. We have to establish optimization models according to specific needs to obtain the "best" solution. For example, for regional mapping, alternative satellite resources and completion time are usually determined in advance, and these do not need planning again. The core requirement for regional mapping is to complete regional imaging on time using as few satellite resources as possible; this core requirement was considered in the proposed model. If insufficient requirements are considered, such as only the coverage gain, for establishing a single-objective model, it will result in wastage of satellite resources, especially in resource-rich cases. Furthermore, if too many requirements are considered in developing the task mission model, the high-dimension objective function will decrease the solution efficiency, or it may be difficult to obtain an optimal solution within the time limit. In short, the "best" solution can be obtained by establishing appropriate models according to different application requirements.

5. Conclusions

We developed a multi-objective modeling method to solve the multi-satellite mission planning problem for large-area mapping considering the following two objective functions: Maximum coverage rate and minimum number of imaging strips. The aim was to cover the entire target region using as few satellite resources as possible. The proposed model takes the imaging strip swing angle and strip selection as the two decision variables. It can integrate regional decomposition and satellite resource allocation into the planning model. By solving the model, the satellite configuration scheme and side sway scheme of the imaging strip can be obtained directly, which simplifies the satellite planning process. We used NSGA-II to solve the model and used the Vatti algorithm to calculate the effective coverage area of the imaging strips, thus improving the efficiency of the model solution. Compared to the single-objective model, which only takes the coverage rate as the target function, the multi-objective model proposed in this paper can complete regional target imaging and efficiently utilize satellite resources simultaneously. The research results presented in this paper can serve as a reference for developing satellite imaging schemes in rapid regional mapping using satellite resources efficiently.

As for future work, there is considerable scope for further research into multi-objective modeling methods considering imaging quality variations caused by swing angles; this will ensure that the optimal mission scheme meets the mapping quality requirements better.

Author Contributions: X.S. and Y.C. developed the concept and method; X.S. and Y.C. conceived and designed the experiments; Y.C., Z.L. and J.X. performed the experiments; Y.C. and X.S. wrote the paper; M.X. and G.Z. helped in performing the investigations and reviewed the paper. All authors have read and agreed to the published version of the manuscript.

Funding: This paper was supported by the National Key Research and Development Program of China (No. 2016YFB0500801).

Acknowledgments: The authors are also grateful for the constructive comments and suggestions of the manuscript reviewers. We would like to thank Editage (www.editage.cn) for English language editing services.

Conflicts of Interest: The authors declare no conflict of interest.

Appendix A

Table A1. Expanded visible time window of Hubei.

Satellite	Number	Expanded Visible Time Window	Duration
GF1	3	12 September 2019 03:37:18.941–12 September 2019 03:38:39.901	80.960
		16 September 2019 03:34:51.401–16 September 2019 03:36:12.403	81.002
		20 September 2019 03:32:23.699–20 September 2019 03:33:44.725	81.026
GF6	4	10 September 2019 03:33:46.385–10 September 2019 03:35:07.243	80.859
		14 September 2019 03:31:29.512–14 September 2019 03:32:50.443	80.931
		18 September 2019 03:29:12.568–18 September 2019 03:30:33.571	81.003
		19 September 2019 03:52:40.505–19 September 2019 03:54:00.201	79.696
ZY1–02C	4	11 September 2019 01:17:00.897–11 September 2019 01:18:23.889	82.992
		14 September 2019 01:13:42.526–14 September 2019 01:15:05.614	83.088
		16 September 2019 01:44:25.559–16 September 2019 01:45:47.622	82.063
		19 September 2019 01:41:06.266–19 September 2019 01:42:28.497	82.231
ZY3	3	12 September 2019 03:19:10.091–12 September 2019 03:20:28.217	78.126
		13 September 2019 03:00:11.298–13 September 2019 03:01:29.688	78.391
		17 September 2019 03:17:27.763–17 September 2019 03:18:45.976	78.212

Table A2. Expanded visible time window of Finland.

Satellite	Number	Expanded Visible Time Window	Duration
GF1	9	8 September 2019 10:00:14.265–8 September 2019 10:03:09.047	174.782
		9 September 2019 10:23:25.722–9 September 2019 10:26:11.073	165.351
		10 September 2019 10:46:43.096–10 September 2019 10:49:20.435	157.340
		12 September 2019 09:57:48.448–12 September 2019 10:00:44.292	175.844
		13 September 2019 10:20:59.211–13 September 2019 10:23:45.478	166.267
		14 September 2019 10:44:15.999–14 September 2019 10:46:54.146	158.147
		16 September 2019 09:55:22.655–16 September 2019 09:58:19.535	176.880
		17 September 2019 10:18:32.705–17 September 2019 10:21:19.856	167.152
		18 September 2019 10:41:48.935–18 September 2019 10:44:27.822	158.886
GF6	9	8 September 2019 10:43:08.488–8 September 2019 10:45:46.641	158.153
		10 September 2019 09:54:18.108–10 September 2019 09:57:16.020	177.912
		11 September 2019 10:17:31.957–11 September 2019 10:20:19.875	167.918
		12 September 2019 10:40:51.761–12 September 2019 10:43:31.165	159.404
		14 September 2019 09:52:03.128–14 September 2019 09:55:02.054	178.926
		15 September 2019 10:15:16.261–15 September 2019 10:18:05.050	168.789
		16 September 2019 10:38:35.506–16 September 2019 10:41:15.636	160.130
		18 September 2019 09:49:48.115–18 September 2019 09:52:48.063	179.948
		19 September 2019 10:13:00.508–19 September 2019 10:15:50.182	169.673
ZY1-02C	10	8 September 2019 07:51:39.850–8 September 2019 07:54:34.406	174.556
		10 September 2019 08:22:06.897–10 September 2019 08:24:50.347	163.450
		11 September 2019 07:48:23.646–11 September 2019 07:51:19.726	176.080
		13 September 2019 08:18:49.345–13 September 2019 08:21:34.044	164.699
		14 September 2019 07:45:07.585–14 September 2019 07:48:05.217	177.632
		15 September 2019 08:49:26.181–15 September 2019 08:52:00.167	153.985
		16 September 2019 08:15:31.884–16 September 2019 08:18:17.867	165.983
		17 September 2019 07:41:51.672–17 September 2019 07:44:50.888	179.216
		18 September 2019 08:46:06.037–18 September 2019 08:48:42.687	156.650
		19 September 2019 08:12:14.516–19 September 2019 08:15:01.808	167.292
ZY3	9	9 September 2019 10:25:25.674–9 September 2019 10:27:48.094	142.420
		10 September 2019 10:06:21.018–10 September 2019 10:08:58.556	157.538
		11 September 2019 09:47:28.819–11 September 2019 09:50:13.423	164.604
		12 September 2019 09:28:40.879–12 September 2019 09:31:33.524	172.645
		14 September 2019 10:23:37.852–14 September 2019 10:26:07.000	149.148
		15 September 2019 10:04:39.481–15 September 2019 10:07:17.668	158.187
		16 September 2019 09:45:47.459–16 September 2019 09:48:32.812	165.353
		17 September 2019 09:26:59.793–17 September 2019 09:29:53.281	173.489
		19 September 2019 10:21:54.659–19 September 2019 10:24:25.000	150.342

Table A3. Expanded visible time window of Congo.

Satellite	Number	Expanded Visible Time Window	Duration
GF1	10	8 September 2019 08:40:19.703–8 September 2019 08:45:29.891	310.188
		9 September 2019 09:03:41.072–9 September 2019 09:08:49.811	308.739
		10 September 2019 09:27:03.475–10 September 2019 09:32:07.550	304.076
		11 September 2019 09:50:27.151–11 September 2019 09:55:23.367	296.216
		13 September 2019 09:01:13.590–13 September 2019 09:06:22.381	308.791
		14 September 2019 09:24:35.838–14 September 2019 09:29:40.284	304.446
		15 September 2019 09:47:59.330–15 September 2019 09:52:56.237	296.906
		17 September 2019 08:58:45.869–17 September 2019 09:03:54.659	308.789
		18 September 2019 09:22:07.955–18 September 2019 09:27:12.721	304.766
		19 September 2019 09:45:31.264–19 September 2019 09:50:28.814	297.550
GF6	10	8 September 2019 09:23:24.587–8 September 2019 09:28:27.705	303.118
		9 September 2019 09:46:51.121–9 September 2019 09:51:46.372	295.251
		10 September 2019 08:34:18.454–10 September 2019 08:39:27.037	308.583
		11 September 2019 08:57:42.552–11 September 2019 09:02:50.557	308.006
		12 September 2019 09:21:07.670–12 September 2019 09:26:11.328	303.658
		13 September 2019 09:44:34.046–13 September 2019 09:49:30.159	296.113
		15 September 2019 08:55:25.678–15 September 2019 09:00:33.884	308.205
		16 September 2019 09:18:50.663–16 September 2019 09:23:54.851	304.187
		17 September 2019 09:42:16.879–17 September 2019 09:47:13.856	296.978
		19 September 2019 08:53:08.732–19 September 2019 08:58:17.126	308.393
ZY1-02C	10	8 September 2019 06:29:19.755–8 September 2019 06:34:37.655	317.899
		9 September 2019 07:34:00.284–9 September 2019 07:39:05.034	304.749
		10 September 2019 06:59:59.710–10 September 2019 07:05:14.488	314.778
		11 September 2019 06:26:01.584–11 September 2019 06:31:19.506	317.923
		12 September 2019 07:30:41.590–12 September 2019 07:35:47.747	306.157
		13 September 2019 06:56:41.292–13 September 2019 07:01:56.746	315.454
		15 September 2019 07:27:22.861–15 September 2019 07:32:30.339	307.479
		16 September 2019 06:53:22.827–16 September 2019 06:58:38.867	316.040
		18 September 2019 07:24:04.089–18 September 2019 07:29:12.804	308.715
		19 September 2019 06:50:04.313–19 September 2019 06:55:20.846	316.533
ZY3	10	8 September 2019 09:26:53.909–8 September 2019 09:31:41.497	287.588
		9 September 2019 09:07:54.501–9 September 2019 09:12:48.422	293.922
		10 September 2019 08:48:55.894–10 September 2019 08:53:54.108	298.214
		11 September 2019 08:29:57.981–11 September 2019 08:34:58.421	300.439
		13 September 2019 09:25:12.383–13 September 2019 09:30:00.707	288.324
		14 September 2019 09:06:12.876–14 September 2019 09:11:07.342	294.466
		15 September 2019 08:47:14.162–15 September 2019 08:52:12.726	298.564
		16 September 2019 08:28:16.126–16 September 2019 08:33:16.720	300.594
		18 September 2019 09:23:29.924–18 September 2019 09:28:18.957	289.033
		19 September 2019 09:04:30.312–19 September 2019 09:09:25.300	294.988

References

1. Campbell, J.B.; Wynne, R.H. *Introduction to Remote Sensing*; Guilford Press: New York, NY, USA, 2011.
2. El Garouani, A.; Mulla, D.J.; El Garouani, S.; Knight, J. Analysis of urban growth and sprawl from remote sensing data: Case of Fez, Morocco. *Int. J. Sustain. Built Environ.* **2017**, *6*, 160–169. [CrossRef]
3. Gao, Z.; Zhou, X. Cause Analysis and Accuracy Improvement of Confusing Land Cover Types in China Geography Census. In Proceedings of the Third International Conference on Agro-Geoinformatics, Beijing, China, 11–14 August 2014; pp. 1–5.
4. Khalid, N.; Ullah, S.; Ahmad, S.S.; Ali, A.; Chishtie, F. A remotely sensed tracking of forest cover and associated temperature change in Margalla hills. *Int. J. Digit. Earth* **2019**, *12*, 1133–1150. [CrossRef]
5. Wang, J.; Zhu, X.; Qiu, D.; Yang, L.T. Dynamic scheduling for emergency tasks on distributed imaging satellites with task merging. *IEEE Trans. Parallel Distrib. Syst.* **2013**, *25*, 2275–2285. [CrossRef]

6. Havivi, S.; Schvartzman, I.; Maman, S.; Rotman, S.; Blumberg, D. Combining TerraSAR-X and Landsat Images for Emergency Response in Urban Environments. *Remote Sens.* **2018**, *10*, 802. [CrossRef]
7. Jiang, Y.; Zhang, G.; Wang, T.; Li, D.; Zhao, Y. In-Orbit Geometric Calibration without Accurate Ground Control Data. *Photogramm. Eng. Remote Sens.* **2018**, *84*, 485–493. [CrossRef]
8. Zhai, X.; Niu, X.; Tang, H.; Wu, L.; Shen, Y. Robust satellite scheduling approach for dynamic emergency tasks. *Math. Probl. Eng.* **2015**, *2015*. [CrossRef]
9. Hu, Q. High-efficiency mission planning and distribution system of the land observation satellites. *Glob. J. Res. Eng.* **2015**. Available online: https://www.researchgate.net/publication/276264173_High-Efficiency_Mission_Planning_and_Distribution_System_of_the_Land_Observation_Satellites (accessed on 20 January 2020). [CrossRef]
10. Wu, Z.; Li, L.; Li, Y.; Gao, Y. Simulation of Two-Satellite Reconnaissance System with Intelligent Decision Based on Object Detection. In Proceedings of the Chinese Control and Decision Conference (CCDC), Nanchang, China, 3–5 June 2019; pp. 2130–2135.
11. Ji, H.; Huang, D. A mission planning method for multi-satellite wide area observation. *Int. J. Adv. Rob. Syst.* **2019**, *16*. [CrossRef]
12. Galán-Vioque, J.; Vázquez, R.; Carrizosa, E.; Vera, C.; Perea, F.; Martín, F. Towards a visual tool for swath acquisition planning in multiple-mission eoss. In Proceedings of the IWPSS 2011 Workshop Proceedings, Freiburg, Germany, 11–16 June 2011.
13. Taitus. Savoir: Swath Acquisition Viewer. 2011. Available online: www.taitussoftware.com (accessed on 10 November 2019).
14. Bai, G. Regional Mission Survey Satellite Planning Method and Application Research. Master's Thesis, National University of Defense Technology, Changsha, China, 2009.
15. He, R.; Li, J.; Yao, F.; Xing, L. *Mission Planning Technology for Imaging Satellites*; Science Press: Beijing, China, 2011.
16. Rivett, C.; Pontecorvo, C. *Improving Satellite Surveillance through Optimal Assignment of Assets*; Defence Science and Technology Organisation: Edinburgh, Australia, 2003.
17. Ruan, Q. Research on the Scheduling of Imaging Reconnaissance Satellites for Regional Targets. Ph.D. Thesis, National University of Defense Science and Technology, Changsha, China, 2006.
18. Shao, X.; Zhang, Z.; Wang, J.; Zhang, D. NSGA-II-based multi-objective mission planning method for satellite formation system. *J. Aerosp. Technol. Manag.* **2016**, *8*, 451–458. [CrossRef]
19. Li, J. Multi-Satellite collaborative ground observation mission planning for regional targets. *Sci. Surv. Mapp.* **2008**, *33*, 54–56.
20. Liu, X.; Chen, Y.; Long, Y. A MapX-based preprocessing approach for multi-satellite cooperative observation towards area target. *Syst. Eng. Theory Pract.* **2010**, *30*, 2269–2275.
21. Yanchao, H.; Ming, X.; Zhi, Y.; Shengli, L. Scheduling Imaging Mission for Area Target Based on Satellite Constellation. In Proceedings of the 27th Chinese Control and Decision Conference (2015 CCDC), Qingdao, China, 23–25 May 2015; pp. 3225–3230.
22. He, C.; Zhu, X.; Qiu, D. Multi-satellite collaborative scheduling method for emergency imaging observation tasks. *Syst. Eng. Electron.* **2012**, *34*, 726–731.
23. Shi, L.; Huang, P.; Zhan, Y.; Zhu, Z.; Ma, G. Application of approximation algorithm to regional target imaging mission planning for optical remote sensing satellites. *Spacecr. Eng.* **2017**, *26*, 7–13.
24. Liu, S.; Hodgson, M.E. Satellite image collection modeling for large area hazard emergency response. *ISPRS J. Photogramm. Remote Sens.* **2016**, *118*, 13–21. [CrossRef]
25. Perea, F.; Vazquez, R.; Galan-Viogue, J. Swath-acquisition planning in multiple-satellite missions: An exact and heuristic approach. *IEEE Trans. Aerosp. Electron. Syst.* **2015**, *51*, 1717–1725. [CrossRef]
26. De Elia, E.; Oglietti, M.; Masuelli, S.; Romero, E. *Planning of Satellite Images Applied to Early Warning Hydrological Models*; CONAE—Argentine National Space Agency: Paseo Colón, Argentina, 2013.
27. Li, X.-M. Two-Archive2 Algorithm for Large-Scale Polygon Targets Observation Scheduling Problem. In Proceedings of the 2nd International Conference on Information Technology and Management Engineering, Shanghai, China, 23–24 April 2017.
28. Niu, X.; Tang, H.; Wu, L. Satellite scheduling of large areal tasks for rapid response to natural disaster using a multi-objective genetic algorithm. *Int. J. Disaster Risk Reduct.* **2018**, *28*, 813–825. [CrossRef]

29. Cui, J.; Zhang, X. Application of a multi-satellite dynamic mission scheduling model based on mission priority in emergency response. *Sensors* **2019**, *19*, 1430. [CrossRef]
30. Hao, H. Research on Modeling and Solving Methods of Agile Satellite Mission Planning. Ph.D. Thesis, Harbin University of Technology, Harbin, China, 2013.
31. Zitzler, E.; Laumanns, M.; Thiele, L. SPEA2: Improving the strength pareto evolutionary algorithm. *TIK-Report* **2001**, *103*. [CrossRef]
32. Deb, K.; Pratap, A.; Agarwal, S.; Meyarivan, T. A fast and elitist multiobjective genetic algorithm: NSGA-II. *IEEE Trans. Evolut. Comput.* **2002**, *6*, 182–197. [CrossRef]
33. Corne, D.W.; Jerram, N.R.; Knowles, J.D.; Oates, M.J. PESA-II: Region-Based Selection in Evolutionary Multiobjective Optimization. In Proceedings of the 3rd Annual Conference on Genetic and Evolutionary Computation, San Francisco, CA, USA, 7–11 July 2001; pp. 283–290.
34. Zheng, J. *Multi-Objective Evolutionary Algorithm and its Application*; Science Press: Beijing, China, 2007; pp. 2–11.
35. Vatti, B.R. A generic solution to polygon clipping. *Commun. ACM* **1992**, *35*, 56–63. [CrossRef]
36. Max, K.A. *Computer Graphics and Geometric Modelling: Implementation and Modelling*; Springer: Berlin/Heidelberg, Germany, 2005.
37. Li, S.; Shen, X.; Yao, H.; Zhang, G.; Liu, Y. Optimization method of satellite swing angle for regional imaging mission. *J. Wuhan Univ.* **2019**, *44*, 593–600.